Versican provides the provisional matrix for uterine spiral artery dilation and fetal growth

Yusuke Sagae [a], Akihito Horie [a], Akihiro Yanai [a], Tsutomu Ohara [a], Baku Nakakita [a], Yoshimi Kitawaki [a], Asuka Okunomiya [a], Hirohiko Tani [b], Ken Yamaguchi [a], Junzo Hamanishi [a], John P. Lydon [c], Takiko Daikoku [d], Hideto Watanabe [e] and Masaki Mandai [a]

***a* - Department of Gynecology and Obstetrics,** *Kyoto University Graduate School of Medicine, Kyoto, Japan*
***b* - Department of Gynecology and Obstetrics,** *Shizuoka General Hospital, Shizuoka, Japan*
***c* - Department of Pathology and Immunology, Center for Drug Discovery, Center for Reproductive Medicine,** *Baylor College of Medicine, Houston, TX, United States of America*
***d* - Division of Animal Disease Model, Research Center for Experimental Modeling of Human Disease,** *Kanazawa University, Kanazawa, Japan*
***e* - Institute for Molecular Science of Medicine, Aichi Medical University,** *Nagakute, Japan*

Corresponding author. *a_horie@kuhp.kyoto-u.ac.jp.*
https://doi.org/10.1016/j.matbio.2022.11.004

Abstract

The extracellular matrix (ECM) in the endometrium plays a crucial role in mammalian pregnancy. We have shown that versican secreted from the endometrial epithelium promotes embryo implantation. Versican is a proteoglycan, a major player in the provisional matrix, and versikine, its N-terminal fragment cleaved by ADAMTS proteinases, serves as a bioactive molecule. Here, since versican expression in the placenta was dynamically altered in humans and mice, we investigated the role of versican in pregnancy using uterine-specific *Vcan* deletion mice (uKO mice) and ADAMTS-resistant versican expressing mice (V1R mice). uKO mice exhibited insufficient spiral artery dilation, followed by fetal growth restriction and maternal hypertension. Further analysis revealed impaired proliferation of tissue-resident natural killer cells required for spiral artery dilation. V1R mice showed the same results as the control, eliminating the involvement of versikine. Our results provide a new concept that versican, one factor of ECM, contributes to placentation and following fetal growth.

Introduction

From embryo implantation to early placentation, the endometrium is an important organ for the reception of the embryo [1,2]. Endometrial abnormalities lead to implantation failure, repeated miscarriages, and a spectrum of poor obstetric outcomes, including early-onset preeclampsia, severe fetal growth restriction (FGR), preterm premature rupture of membranes, intrauterine fetal death, and placental abruption [1,2]. Various factors contribute to endometrial receptivity, including hormones such as progesterone, transcription factors such as C/EBPβ, Hoxa10, Msx1, and Msx2, and biochemical factors such as LIF, COX2, and IFN-γ. Immune cells, such as regulatory T cells, uterine natural killer (NK) cells, and M2 macrophages, are also involved in this process [3−5]. For example, NK cells, abundant in the implantation sites [6−8], secrete IFN-γ and dilate the spiral arteries, thereby providing sufficient blood flow necessary for fetal development [6,9-12].

The extracellular matrix (ECM) consists of collagens, fibronectin, laminins, elastin, hyaluronan, and proteoglycans [13] and provides an appropriate environment for these factors, and therefore is crucial for embryo implantation. Its abnormalities cause implantation failure, repeated miscarriages, and severe

pregnancy complications [3]. As the ECM of the endometrium alters dynamically from implantation to early placentation, it could exert a critical function in this process [14].

Versican is a chondroitin sulfate (CS) proteoglycan, playing an important role in the formation of the provisional matrix [15], which enables dynamic transformations of the ECM. Its core protein consists of an N-terminal G1 domain, a C-terminal G3 domain, and two CS-attachment domains, CS-α and CS-β, between the G1 and G3 domains. There were four classical isoforms: V0 (G1-CSα-CSβ-G3), V1 (G1-CSβ-G3), V2 (G1-CSα-G3), and V3 lacking CS chains (G1-G3) [16]. Later, another isoform, V4 (G1 portion of CSβ-G3), was found in human breast cancer [17]. The G1 domain binds hyaluronan (HA) and regulates HA-mediated signaling. The G3 domain binds other ECM molecules, and their complex binds transforming growth factor-β (TGFb) and bone morphogenetic proteins (BMPs). The CS chains with a negative charge bind positively charged growth factors and cytokines [18]. With these moieties, versican regulates cellular processes such as migration, invasion, proliferation, and apoptosis during organogenesis and in pathological conditions such as inflammatory diseases and cancers [19,20]. In addition, the versican core protein is cleaved by ADAMTS proteinases, and the N-terminal fragment has been shown to serve as a bioactive molecule termed versikine. Previously we demonstrated that versican expression in human endometrium is regulated by ovarian steroids, and that versican secreted from the endometrial epithelium during the luteal phase promotes embryo implantation [13]. However, the roles of versican and versikine during pregnancy have not been understood.

Here, we investigated the role of versican in the endometrial stroma in the process of placentation, using uterine-specific versican deletion mice uKO and versican knockin mice termed V1R, whose versican is resistant to ADAMTS cleavage. We found that versican contributes to the proliferation of NK cells, facilitating the dilation of spiral arteries and enabling adequate placentation and fetal growth.

Results

Distribution of versican in the pregnant uterus of humans and mice

First, we examined the expression of versican in the placenta. In the human placenta of the first trimester, versican was present throughout the decidual ECM except in the vicinity of the anchoring villi (Fig. 1A). In the second trimester, it was abundant on the maternal side of the decidual ECM, whereas it was absent in the fibrinoid area on the fetal side (Fig. 1B). In the third trimester, versican was hardly detected in the decidua (Fig. 1C). Then, we examined versican expression in murine placenta during pregnancy (diagram shown in Supplemental Figure 1). Versican was distributed throughout the endometrial stroma in estrus and at day 4 of pregnancy (i.e., embryonic day 3.5, hereafter denoted by days of pregnancy) (Fig. 1D, E). At day 5, whereas versican decreased from the vicinity of the embryo, which became remarkable at day 6, it remained in the endometrial stroma (Fig. 1F, G). At day 8, versican was condensed on the mesometrial side, where placental formation begins (Fig. 1H). At day 10, it was detected in the myometrium but not in the decidua (Fig. 1I). At days 8 and 10, versican was absent in the vascular smooth muscle of spiral arteries (Fig. 1J, K). In humans and mice, versican was abundant on the placental formation side until midterm pregnancy. RT-qPCR using mRNA extracted from the whole uterus and implantation sites showed that *Vcan* and *Adamts-1* and *9* were significantly upregulated at day 6 compared to estrus and that V1 was dominant in *Vcan* isoforms (Supplemental Fig. 2).

Pregnancy outcome in uterine-specific *Vcan* deletion mice (uKO mice)

To examine the role of versican in pregnancy, we generated uterine-specific *Vcan* deletion mice (uKO mice) by crossing *Pgr*-Cre mice with *Vcan*-floxed mice (Supplemental Fig. 3A) and analyzed them. qRT-PCR with primers designed to detect exon 2, common to all Vcan isoforms, confirmed little mRNA for the *Vcan* gene in the whole non-pregnant uterus of uKO mice (Supplemental Fig. 3B). Immunohistochemistry showed no expression of versican in the endometrial stroma or myometrium of non-pregnant uKO mice (Supplemental Fig. 3C). We also confirmed little versican expression in the endometrium and decidua of uKO mice at any stage of pregnancy (Supplemental Fig. 3C). In contrast, HA was detected in both uKO and control uterus (Supplemental Fig. 3D).

When compared between uKO and control mice at day 18, there were no significant differences in the pregnancy rate (p = 0.8572, Fig. 2A). Although there was a tendency for a higher percentage of uKO mice to have miscarriages (uKO: 60%, control: 20%, p = 0.0679), there was no significant difference in the incidence of miscarriages per mother (p = 0.1762, Fig. 2B), or in the number of live pups per mother (p = 0.0686, Fig. 2C). In contrast, the average pup weight was significantly smaller (p = 0.0053, Fig. 2D, E, F) in uKO mice, although no abnormal phenotypes were found in them (Fig. 2D, E) and there was no difference in the mean placental weight per mother (p = 0.6212, Fig. 2G). The maternal blood pressure at day 18 was significantly higher

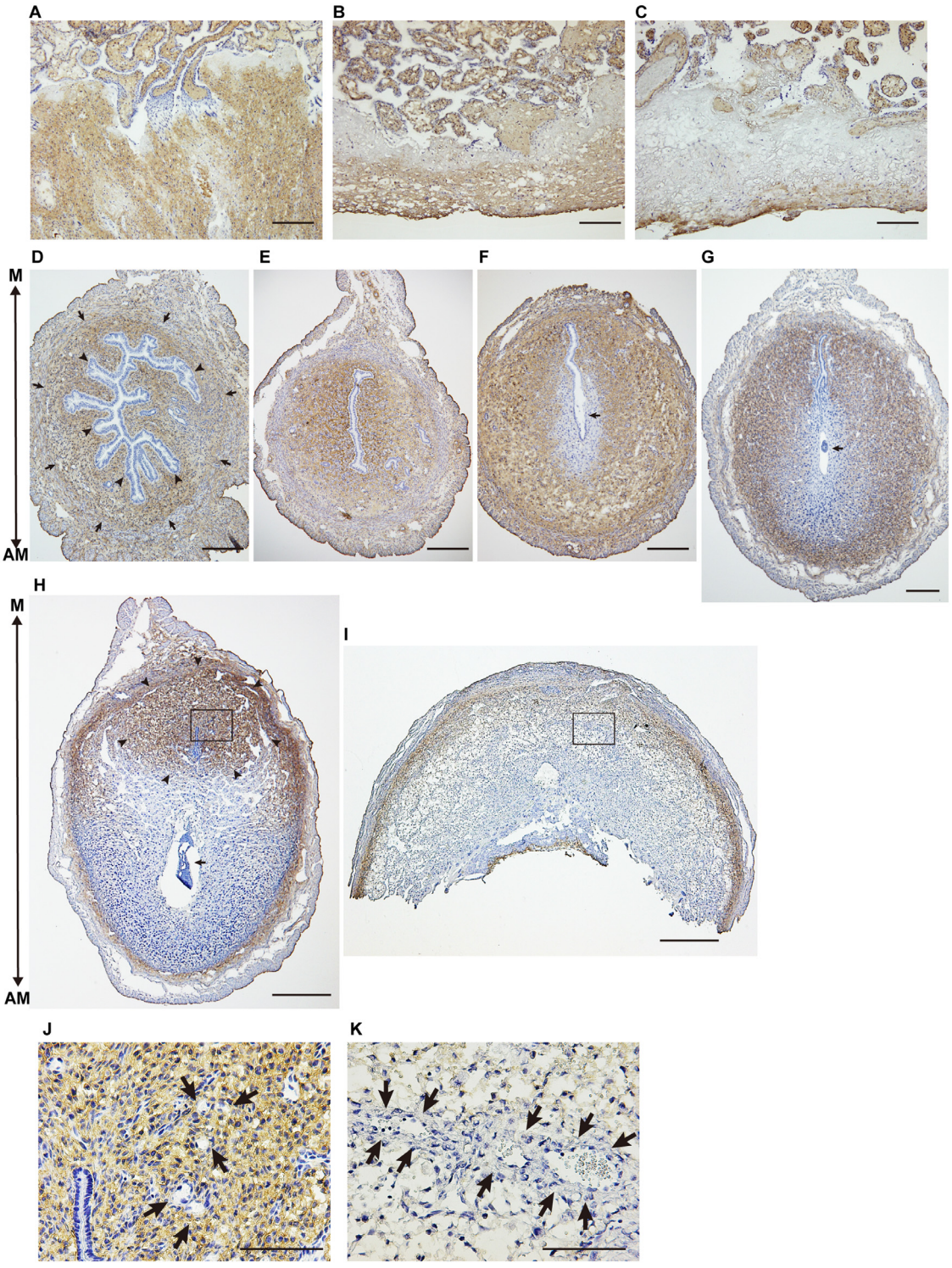

Fig. 1. The expression and distribution of versican in the uterus during pregnancy in humans and mice.
(A-C) Distribution of versican in human implantation site and placenta. The upper side is the fetal side (chorion), and the lower side is the maternal side (decidua) in every panel; scale bar = 500 μm. (A) Implantation site in the first trimester of pregnancy (10 weeks of gestation). (B) Placenta in the second trimester (18 weeks of gestation). (C) Placenta in the third trimester (30 weeks of gestation). (D-I) Distribution of versican in murine implantation sites. The upper side is the mesometrial side (M), and the lower side is the antimesometrial side (AM) in every panel. (D) Estrus, (E) day 4, (F) day 5, and (G) day 6. (D-G) Scale bar = 200 μm. (F-H) Arrows indicate the embryos. (H) Day 8; arrowheads indicate the area where versican was kept in decidua on the mesometrial side. (I) Day 10. (H, I) Scale bar = 500 μm. (J) Magnified image of the square part in (H). (K) Magnified image of the square part in (I). (J, K) arrows indicate vascular smooth muscle of spiral arteries, where versican was not detected.

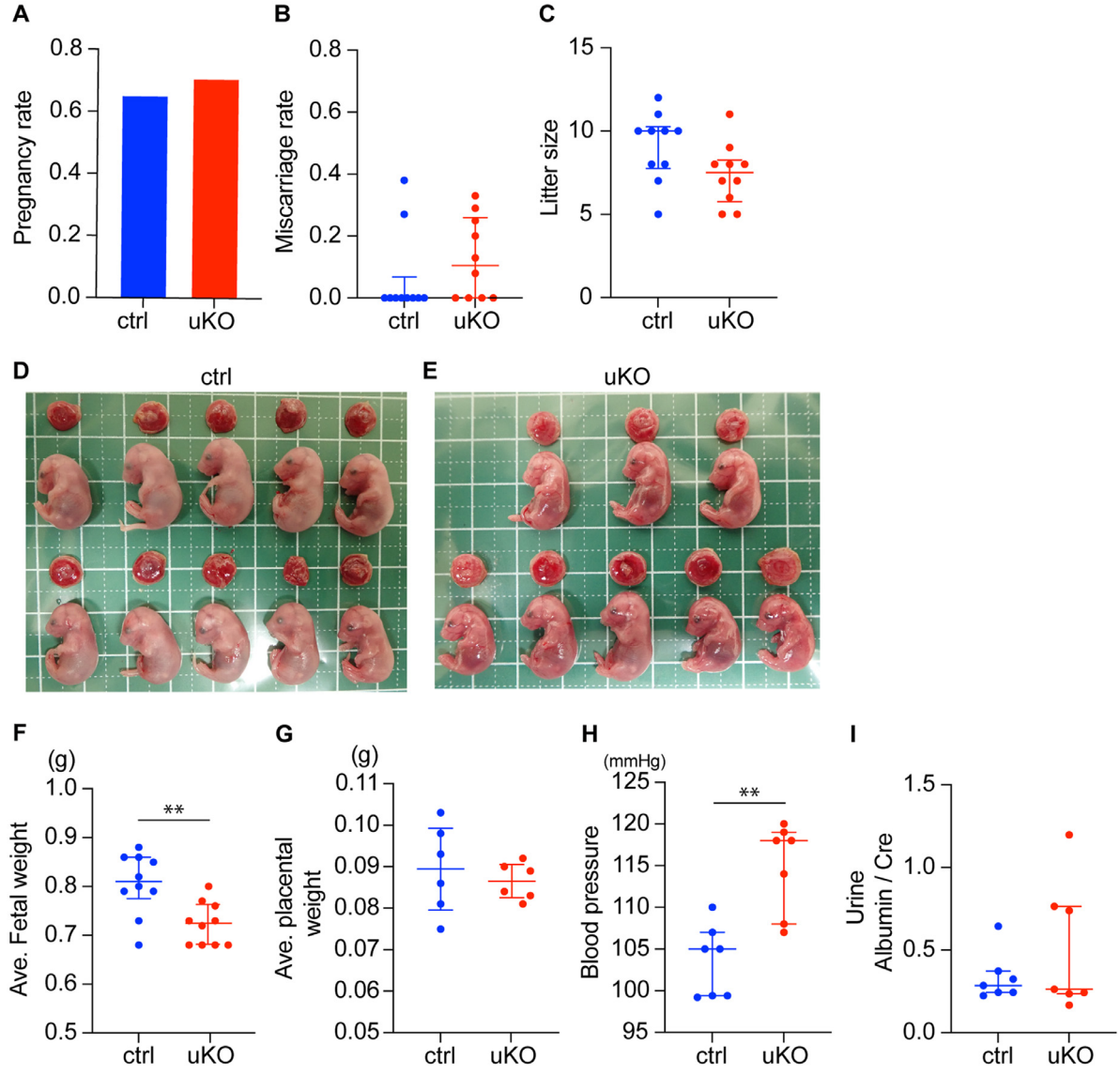

Fig. 2. Pregnancy outcome of uKO and control mice at day 18

Pregnancy outcomes when uKO and control females were mated with wild-type males. (A) Pregnancy rate, i.e., the rate of pregnant mice to plug-positive mice. The difference was analyzed using chi-square test. ctrl, $n = 23$; uKO, $n = 24$. $p = 0.852$ (B) Miscarriage rate; the rate of miscarriage relative to the implantation sites found in the pregnant murine uterus; $n = 10$, $p = 0.1762$. (C) Litter size; $n = 10$, $p = 0.757$. (D, E) Representative pictures of fetuses and placentas from control mice (D) and uKO mice (E). (F) Average fetal weight per pregnant mouse; $n = 10$, $p = 0.0053$. (G) Average placenta weight per pregnant mouse; $n = 6$, $p = 0.6212$. (H) Maternal systolic blood pressure at day 18; $n = 7$, $p = 0.0029$. (I) Urinary albumin/Cre ratio in pregnant mice at day 18; $n = 7$, $p = 0.9015$. (B, C, F-I) Differences were analyzed using Mann-Whitney test; median ± interquartile range; $^{*}p < 0.05$, $^{**}p < 0.01$.

ctrl, control mice; uKO, uterine-specific *Vcan* deletion mice.

($p = 0.0029$, Fig. 2H) in uKO mice, despite no difference in the ratio of albumin to creatinine in maternal urine ($p = 0.9015$, Fig. 2I).

Evaluation of fetal weight and placenta at day14 in uKO mice

As these results of pregnancy outcomes suggested that the absence of versican in the uterus causes FGR and maternal hypertension, we tried to determine their onset. At day 14, the average fetal weight per mother was significantly smaller in uKO mice ($p = 0.0159$, Fig. 3A, B), but there was no significant difference in maternal blood pressure ($p = 0.3800$, Fig. 3C). Histologically, the ratio of the area of decidua to the placenta and the ratio of the depth of the mesometrial lymphoid aggregate of pregnancy (MLAp) to placenta were significantly

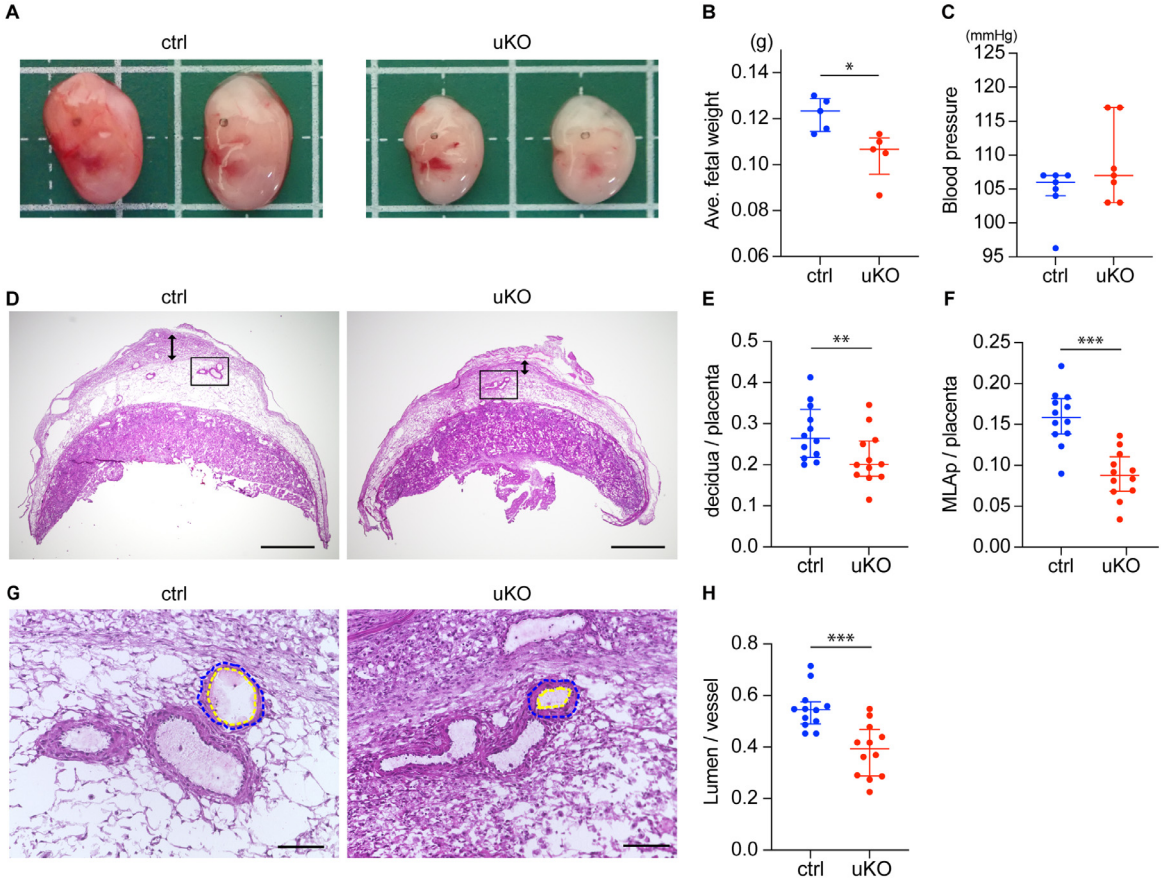

Fig. 3. Evaluation of fetus and placenta at day 14 in control and uKO mice.

(A) Representative image of fetuses in control and uKO mice. (B) Average fetal weight per pregnant mouse; $n = 5$, $p = 0.0159$. (C) Maternal systolic blood pressure during day 13−15; $n = 7$, $p = 0.0380$. (D) Representative H&E-stained histological image of placenta. Arrow indicates MLAp; scale bar = 500 μm (E) The ratio of decidual area to whole placenta area; $p = 0.0242$. (F) The ratio of MLAp depth to whole placenta depth; $p < 0.0001$. (G) Magnified image of the square part in (D). Yellow and blue dotted lines indicate the lumen and wall of the spiral artery, respectively. Scale bar = 100 μm. (H) The ratio of lumen diameter to wall diameter; $p = 0.0005$. (E, F, H) three placentas each were obtained from four mice; $n = 12$.

ctrl, control mice; MLAp, the mesometrial lymphoid aggregate of pregnancy; uKO, uterine-specific *Vcan* deletion mice.

(B, C, E, F, H) Differences were analyzed using Mann-Whitney test; median ± interquartile range; *$p < 0.05$, **$p < 0.01$, ***$p < 0.001$.

smaller in uKO mice (Fig. 3D; $p = 0.0242$, Fig. 3E; $p<0.0001$, Fig. 3F). In addition, the spiral arteries in the decidua of uKO mice exhibited thick vessel walls and narrow lumens (Fig. 3G), which was confirmed by the measurement of diameters of lumen and wall ($p = 0.0005$, Fig. 3H). Since the spiral artery dilation occurs around day 10 [21], we further investigated the weight of the implantation site and the spiral arteries at day 10. The weight of the implantation site was significantly smaller in the uKO group ($p = 0.0286$, Supplemental Fig. 4A, B) and the ratio of their lumen diameter to wall diameter was already smaller in the spiral arteries of uKO mice ($p = 0.0019$, Supplemental Fig. 4C-E).

Evaluation of the implantation site at day 8 in uKO mice

Although versican in the decidua almost disappeared by day 10 (Fig. 1I), it was present at high levels on the mesometrial side at day 8 (Fig. 1H). When we examined the implantation sites at day 8 in detail, the average weight of the implantation site was significantly smaller in the uKO group ($p = 0.0041$, Fig. 4A, B, C). Histologically, whereas the antimesometrial side was similar, the lateral vascular sinus (LVS) and the area of the mesometrial side, where versican is expressed in control mice, were poorly developed in uKO mice (Fig. 4C). On the

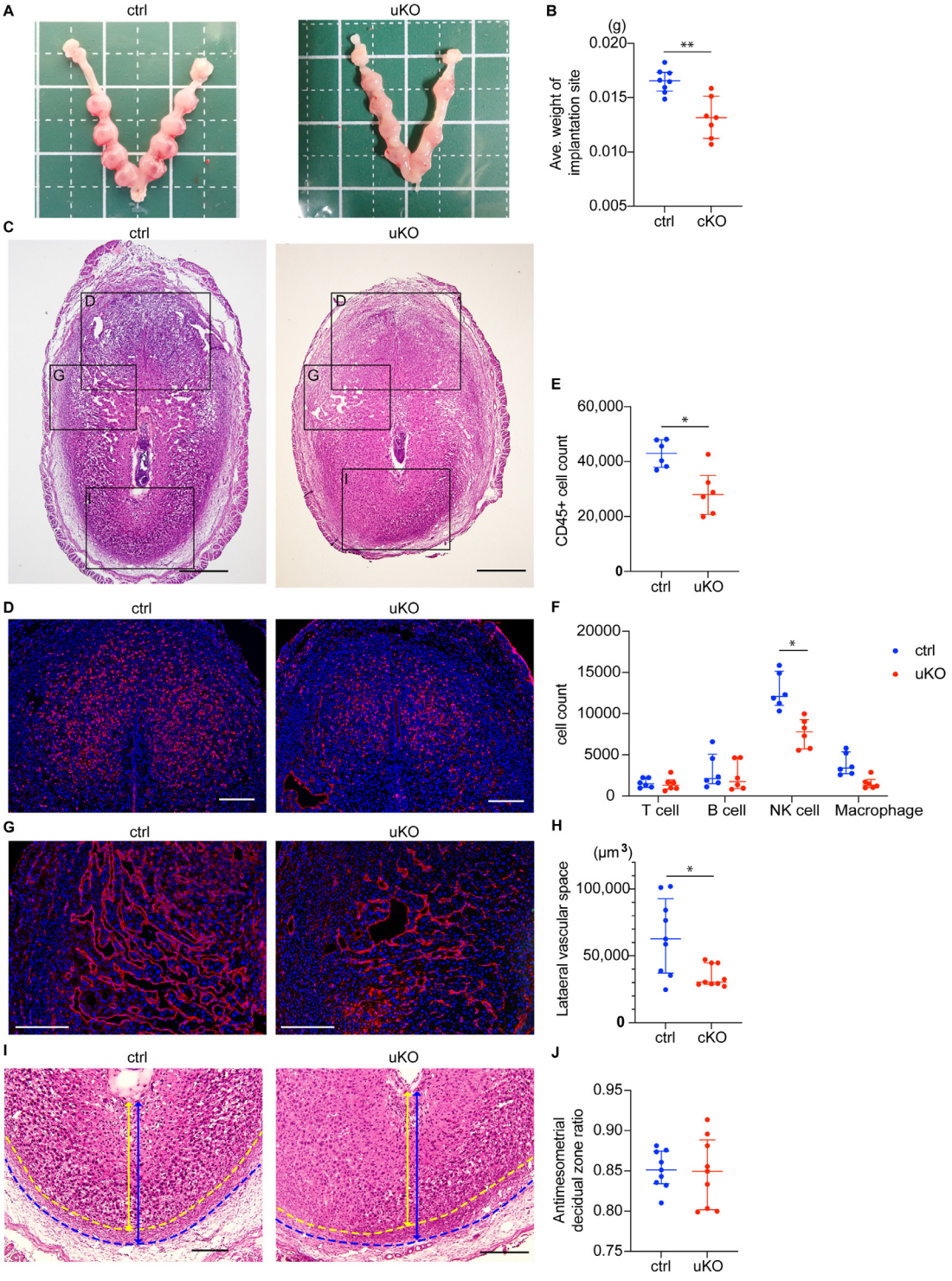

Fig. 4. Evaluation of implantation sites at day 8 in control and uKO mice.

(A) Representative images of the pregnant uterus in control and uKO mice. (B) Average implantation site weight per pregnant mouse; $n = 7$, $p = 0.0041$. (C) Representative H&E-stained histological images of implantation sites. The upper side is the mesometrial side (M), and the lower side is the antimesometrial side (AM). Scale bar = 500 μm. (D) Histological image of the D-marked rectangles in (C) with fluorescent immunostaining for CD45 (red) and DAPI staining for nuclei (blue). Scale bar = 200 μm. (E) CD45 positive cell count per implantation site using flow cytometry. $n = 6$, $p = 0.0152$. (F) Numbers of T cells, B cells, NK cells, and macrophages per implantation site at day 8. $n = 6$; Q value; T cells, 0.5296; B cells, 0.5296; NK cells, 0.00656; macrophages, 0.0131. (G) Histological image of the F-marked rectangles in (C) with

mesometrial side, where lymphocytes were abundant in normal pregnancy [14], immunofluorescence staining showed a decreased number of CD45+ lymphocytes in uKO mice (Fig. 4D), which was confirmed by flow cytometry ($p = 0.0152$, Fig. 4E). Further analysis revealed a significantly lower number of NK cells in CD45+ lymphocytes in uKO mice ($Q = 0.00656$, Fig. 4F). When LVS was analyzed with immunofluorescence staining for CD31 (Fig. 4G), the area of LVS was smaller in uKO mice than in control mice ($p = 0.0228$, Fig. 4H). In contrast, decidualized cells on the antimesometrial side, where versican was absent even in control mice, were similarly distributed in both uKO and control mice ($p = 0.7962$, Fig. 4I, J).

Analysis of NK cells in the implantation sites of uKO mice

To determine how versican deletion causes a decrease in NK cells in the implantation site, we performed a detailed analysis of NK cells. By immunofluorescence staining, many NK cells were observed in the versican-rich area in control mice (Fig. 1D, E, G, H, Fig. 5A-C) as well as in humans (Supplemental Fig. 5). Whereas the number of NK cells was similar between uKO and control mice in the virgin uterus (Fig. 5A), it appeared fewer in implantation sites of uKO mice at days 6, 8, and 10 (Fig. 5B, C, D). Next, we measured the number of NK cells (CD45+, CD3−, CD19−, NK1.1+) per implantation site at days 6, 8, and 10 by flow cytometry, and counted NK cells in CD49a+ and CD49b+ fractions. Although NK cells are often classified as CD49a+ CD49b− tissue-resident NK (trNK) and CD49a− CD49b+ conventional NK (cNK) cells [7,8,22], we designated CD49a+ cells as tissue-resident NK (trNK) cells and CD49a− cells as conventional NK (cNK) cells, since the CD49a+ population were positive for CD49b by day 8 (Fig. 5E, Supplemental Fig. 6A). The overall number of NK cells was significantly lower in the uKO group at days 6 and 8 (day 6, $p = 0.0260$; day 8, $p = 0.0022$; Fig. 5F), but not at day 10 ($p = 0.0649$, Fig. 5F). Among NK cells, the number of trNK cells was significantly lower in uKO mice at days 6, 8, and 10 ($p = 0.0022$, $p = 0.0022$, and $p = 0.0411$, respectively; Fig. 5G), whereas that of cNK cells was similar at days 6, 8, and 10 ($p = 0.9372$, $p = 0.2403$, and $p = 0.8182$, respectively; Fig. 5H). These results indicate that deletion of versican decreases the number of trNK cells in the implantation site.

Cell cycle analysis of trNK cells at day 6 in uKO mice

trNK cells increased approximately two-fold from day 6 to 8 in the control group but not in the uKO group. (Fig. 5G). As trNK cells are reported to proliferate locally in the uterus around day 6 to day 8 [7,8], we examined their proliferation at day 6 (The gating process is shown in Supplemental Fig. 7). Ki-67-based cell cycle analysis revealed that whereas Ki-67 positive cells occupied a large proportion of cells in both groups (Fig. 6A), the percentage of cells in the S phase was significantly lower in uKO mice ($p = 0.0087$, Fig. 6B). Next, to focus on the S phase, we performed cell cycle analysis using BrdU. The percentage of cells in the G1 phase was significantly higher ($p = 0.0260$, Fig. 6C, D), and that in the S phase was significantly lower in uKO mice ($p = 0.0022$, Fig. 6C, D). These results indicate that the decreased number of trNK cells in uKO mice is due to the reduction of cell proliferation.

Analysis of the effect of versikine on NK cells

As the uKO uterus lacks versican, it also lacks versikine, a bioactive cleaved fragment of versican. To determine whether the proliferation of trNK cells was operated by versican or versikine, we performed the same analysis on V1R mice, whose versican is resistant to ADAMTS-cleavage, thereby lacking versikine. Immunostaining confirmed accumulation of versican in the homozygote V1R uterus with essentially the same distribution patterns as the control, and the absence of versikine similar to uKO uterus (Fig. 7A). Flow cytometry analysis revealed that the number of total, trNK, and cNK cells in the homozygote V1R mice was similar to that of control mice. These results suggest that versican, but not versikine, promotes the proliferation of trNK cells in the implantation site (Fig. 7B).

fluorescent immunostaining for CD31 (red), which is positive in new blood vessels, and DAPI staining for nuclei (blue). Scale bar = 200 μm. (H) The area of LVS; 3 placentas were obtained from each of 4 mice for $n = 12$; $p = 0.0228$. (I) Magnified image of the I-marked rectangles in (C). Yellow and blue lines indicate the depth of the decidualized cell layer and entire endometrial stromal cell layer, respectively. (J) Antimesometrial decidual zone ratio, which is the ratio of the depth of the decidualized cell layer to that of the entire endometrial stromal cell layer on the antimesometrial side. Scale bar = 200 μm.

(B, E, H, J) Differences were analyzed using Mann-Whitney test, median ± interquartile range, $^*p < 0.05$, $^{**}p < 0.01$.

(F) Differences were analyzed using multiple Mann-Whitney tests; median ± interquartile range; $^*Q < 0.01$.

ctrl, control mice; MLAp, the mesometrial lymphoid aggregate of pregnancy; LVS, lateral vascular space; uKO, uterine-specific *Vcan* deletion mice.

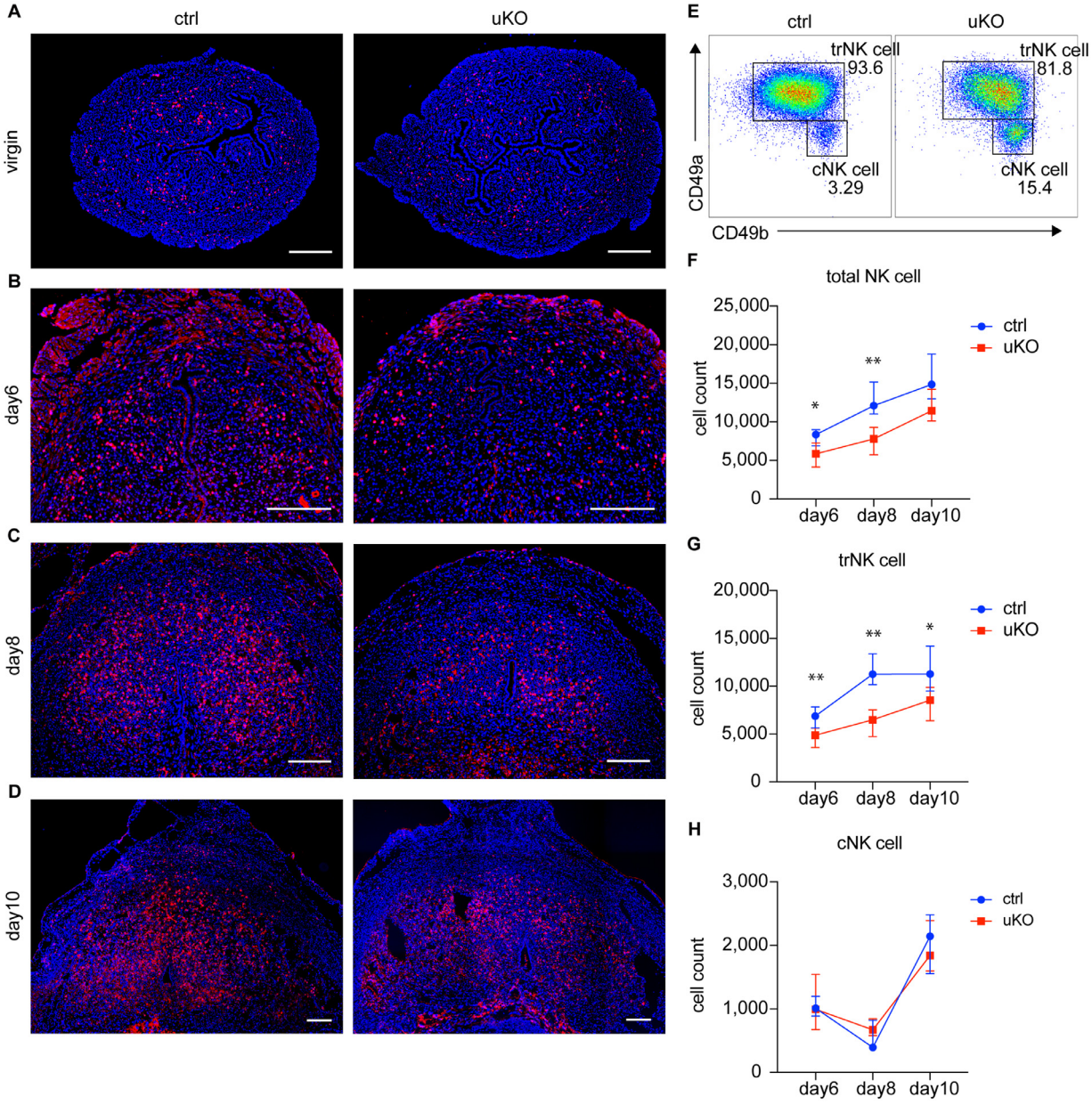

Fig. 5. Analysis of NK cells in the implantation sites in various stages in control and uKO mice.
(A-D) Representative histological images of fluorescent immunostaining of NK1.1 (red) in various stages. The mesometrial side is the upper side on each photo. Nuclei were stained by DAPI (blue). Scale bar = 200 μm. (A) Estrus, (B) day 6, (C) day 8, and (D) day 10. (B-D) The upper side is the mesometrial side. (E) Representative results of flow cytometry analysis on NK cell subpopulation using CD49a and CD49b. (F-H) The transition in the numbers of target cells per implantation site using flow cytometry; $n = 6$ at each stage. Differences were analyzed using Mann-Whitney test on each day between two groups; median ± interquartile range. (F) NK cells on day 6, $p = 0.0260$; day 8, $p = 0.0022$; day 10, $p = 0.0649$. (G) trNK cells on day 6, $p = 0.0022$; day 8, $p = 0.0022$; day 10, $p = 0.0411$. (H) cNK cells on day 6, $p = 0.9372$; day 8, $p = 0.2403$; day 10, $p = 0.8182$. $^{*}p < 0.05$, $^{**}p < 0.01$.

Comparative transcriptomic analysis of implantation sites at day 6

To investigate the mechanism of poor trNK cell proliferation in the uKO uterus, transcriptomic analysis was performed using the implantation sites at day 6. 18,359 genes were detected in the all sample, and 527 genes were identified as differentially expressed genes (DEG) (269 up-regulated genes and 257 down-regulated genes) (Supplemental Fig.

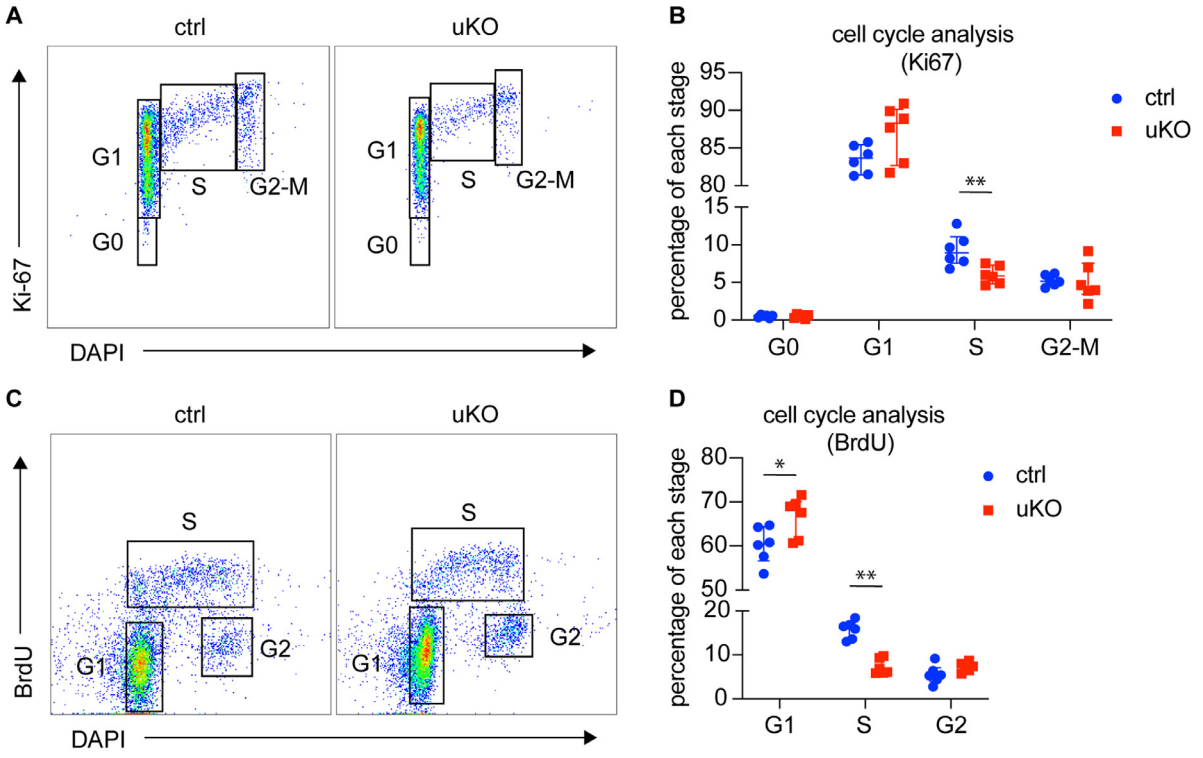

Fig. 6. Cell cycle analysis of trNK cells at day 6 in control and uKO mice.
(A) Representative results of Ki-67-based cell cycle analysis of trNK cells in the implantation site at day 6. (B) The percentage of each stage of cell cycle using anti-Ki-67; $n = 6$. G0, $p = 0.9372$; G1, $p = 0.1320$; S, $p = 0.0087$; G2-M, $p = 0.4848$. (C) Representative results of BrdU-based cell cycle analysis of trNK cells in the implantation site at day 6. (D) The percentage of each stage of cell cycle using BrdU; $n = 6$. G1, $p = 0.0260$; S, $p = 0.0022$; G2, $p = 0.0931$.
(B, D) Differences were analyzed using the Mann-Whitney test in each phase between two groups; median ± interquartile range; $^{*}p < 0.05$, $^{**}p < 0.01$.

8A-C). The results of the GO analysis using these DEG are shown in Table. 1. Among these, when focusing on "female pregnancy," the majority of the genes involved were related to decidualization, such as *Prl* and *Igfbp* (Fig. 8A) [4]. In addition, among the genes constituting the GO term “extracellular matrix”, 24 genes were identified as DEG such as *Tnc, Ogn*, and *Aspn* (Supplemental Fig. 8D).

Genes associated with trNK cells and uterine NK cells were listed from previous reports (Supplemental Table 1). Clustering of the samples by expression of this gene set showed distinct separation into ctrl and uKO (Fig. 8B). *Nfil3, Kitl* and *Pgf*, involved in NK activation and differentiation [6,23-25], and *Ptn, Kit,* and *Vegfc*, expressed in trNK cells [6,23,26], were decreased in uKO mice (Fig. 8C). In summary, the factors involved in decidualization and NK cell activation were altered in uKO mice.

Discussion

In this study, we investigated the distribution and function of versican expressed in the endometrial stroma during pregnancy and revealed several novel findings as follows. First, versican exhibits dynamic and similar expression patterns in humans and mice. Especially, versican was abundant in the mesometrial side in mice, suggesting its involvement in placentation. Second, versican is required to expand spiral arteries, and its deletion causes maternal hypertension and FGR. Third, versican is crucial for the proliferation of trNK cells involved in spiral artery dilation, trophoblast invasion, and immunomodulation. Fourth, these roles are primarily ascribed to intact versican rather than versikine, a bioactive cleaved fragment. Our study provides the concept of how versican as an important player of the provisional matrix contributes to placentation and following fetal growth.

Versican exhibited distinct expression patterns during pregnancy. Before implantation, it was distributed broadly. It gradually disappeared from the vicinity of the embryo, and by day 8, became restricted to the mesometrial side where the placenta was formed. The co-localization of versican and versikine suggests that versican accumulation in the mesometrial side was due to increased expression of

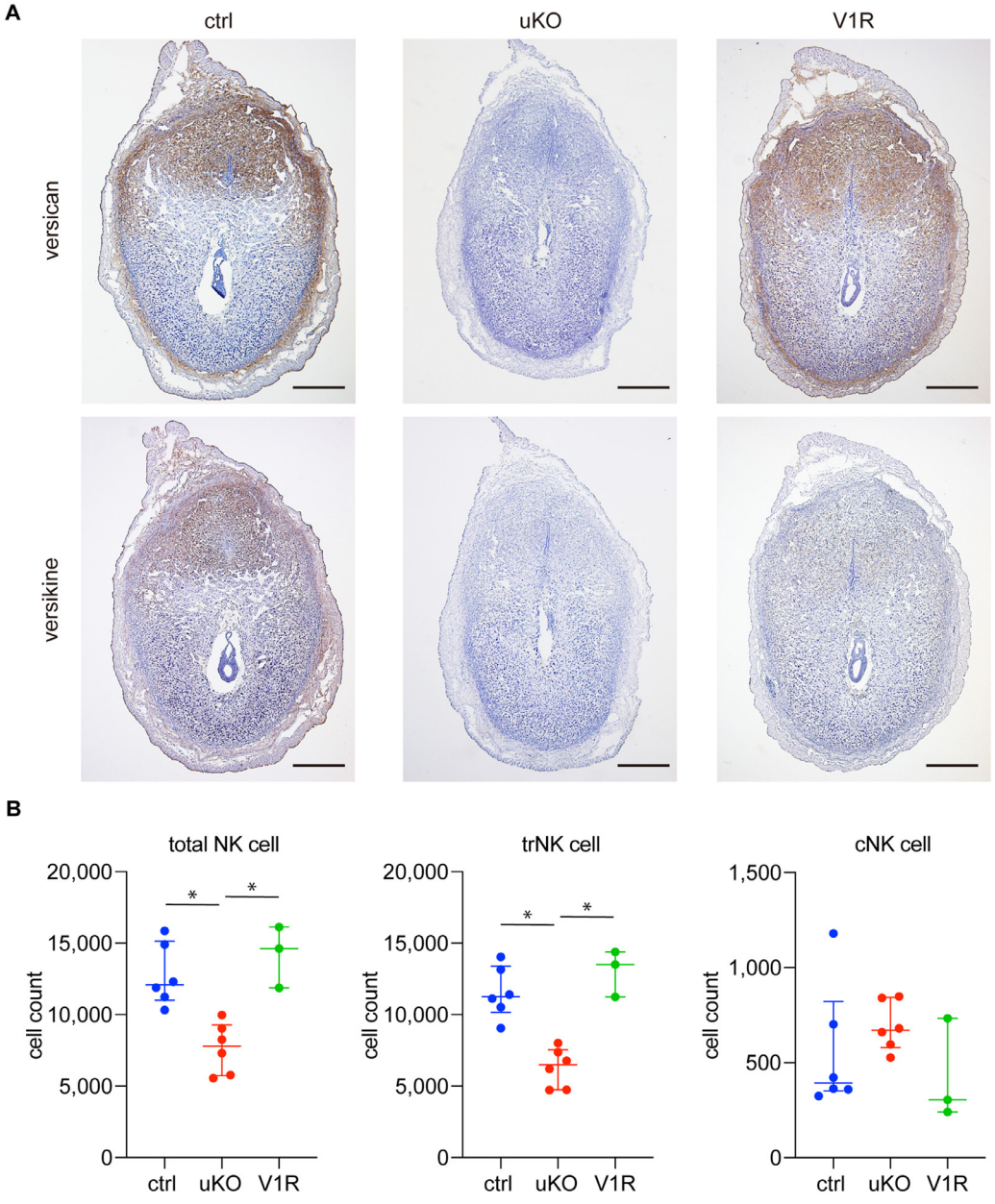

Fig. 7. Analysis of V1R mice at day 8.

(A) Distribution of versican and versikine in murine implantation sites in control, uKO, and V1R mice. The upper side is the mesometrial side (M), and the lower side is the antimesometrial side (AM) in every panel. (B) The number of target cells per implantation site using flow cytometry. ctrl and uKO, $n = 6$; V1R, $n = 3$. Total NK cell, $p = 0.0006$: ctrl vs. uKO, $p = 0.0201$; ctrl vs. V1R, $p > 0.9999$; uKO vs. V1R, $p = 0.0216$. trNK cell, $p = 0.0003$: ctrl vs. uKO, $p = 0.0295$; ctrl vs. V1R, $p > 0.9999$; uKO vs. V1R, $p = 0.0112$. c NK cell, $p = 0.2510$: ctrl vs. uKO, $p = 0.8175$; ctrl vs. V1R, $p > 0.9999$; uKO vs. V1R, $p = 0.3069$.

Differences were analyzed using the Kruskal-Wallis test followed by Dunn's multiple comparison test; median ± interquartile range; $^{*}p < 0.05$, $^{**}p < 0.01$.

versican. As the disappearance of versican correlates with decidualization, a decrease in the extracellular space may prompt its disappearance.

As the number of pups of uKO mice was the same as the control mice, versican is not essential for the establishment and maintenance of pregnancy. In contrast, the deletion of versican caused FGR and maternal hypertension. Detailed analysis of the uKO placenta from the early pregnancy revealed impaired spiral artery dilation at days 10 and 14,

Table. 1. Top 20 terms of biological process in GO analysis of DEG.

	Term name	Adjusted p_value	Term size	intersection size
1	adenylate cyclase-activating G protein-coupled receptor signaling pathway	1.36E-07	144	17
2	synapse organization	2.50E-06	480	28
3	muscle system process	3.18E-06	422	26
4	adenylate cyclase-modulating G protein-coupled receptor signaling pathway	3.63E-06	226	19
5	multi-multicellular organism process	3.63E-05	260	19
6	cell killing	4.02E-05	208	17
7	multi-organism reproductive process	8.00E-05	245	18
8	regulation of signaling receptor activity	9.35E-05	169	15
9	regulation of synapse organization	0.000116	251	18
10	lymphocyte mediated immunity	0.000122	404	23
11	regulation of immune effector process	0.000136	374	22
12	negative regulation of cysteine-type endopeptidase activity	0.000163	107	12
13	regulation of leukocyte mediated cytotoxicity	0.000165	87	11
14	female pregnancy	0.000165	229	17
15	regulation of synapse structure or activity	0.000176	258	18
16	synapse assembly	0.000410	189	15
17	regulation of synapse assembly	0.000442	117	12
18	regulation of leukocyte mediated immunity	0.000520	248	17
19	negative regulation of cysteine-type endopeptidase activity involved in apoptotic process	0.000569	98	11
20	muscle contraction	0.000581	310	19

which is crucial insufficiency to lead to FGR, preeclampsia, and subsequent pregnancy complications [2].

We have revealed a decrease in the NK cells in the mesometrial side of the uKO implantation site around day 6, concomitant with poor proliferation of trNK cells. In mouse models with decreased NK cells exhibit insufficient dilatation of the spiral arteries [10,11,27]. The insufficient spiral artery dilation observed in the uKO placenta is likely due to a decrease in trNK cells.

V1R mice, which lack versikine, showed the same number of NK cells at day 8 as the control mice, indicating that intact versican, not versikine, promotes trNK cell proliferation.

Versican binding HA is considered to exert functions as proteoglycan aggregates [28–31]. HA was observed in the uKO implantation site, indicating versican is dispensable for HA deposition in the ECM. At day 8, versican and HA were essentially co-localized, where NK cells were abundant. Analysis of mice with local HA deficiency in pregnancy will determine whether versican acts as aggregates or as a single molecule. We further examined ECM molecules using our comparative transcriptome and found an increase in *Tnc*, which interacts with versican. Regarding small leucine-rich proteoglycans (SLRPs), we observed increases in *Ogn* and *Aspn* but not *Dcn* and *Bgn. Col1a1, Col3a1*, and *Col5a1*, expressing in the decidua [32], were unaltered.

Our comparative transcriptomic analysis indicated two findings about the poor proliferation of trNK cells. First, expression levels of *Prl* and *Igfbp* [4], involved in decidualization, were decreased significantly. Since the decidualization process includes an increase in uterine natural killer (uNK) cells [14], impaired decidualization may have caused the poor proliferation of trNK cells. Second, the expression levels of the trNK

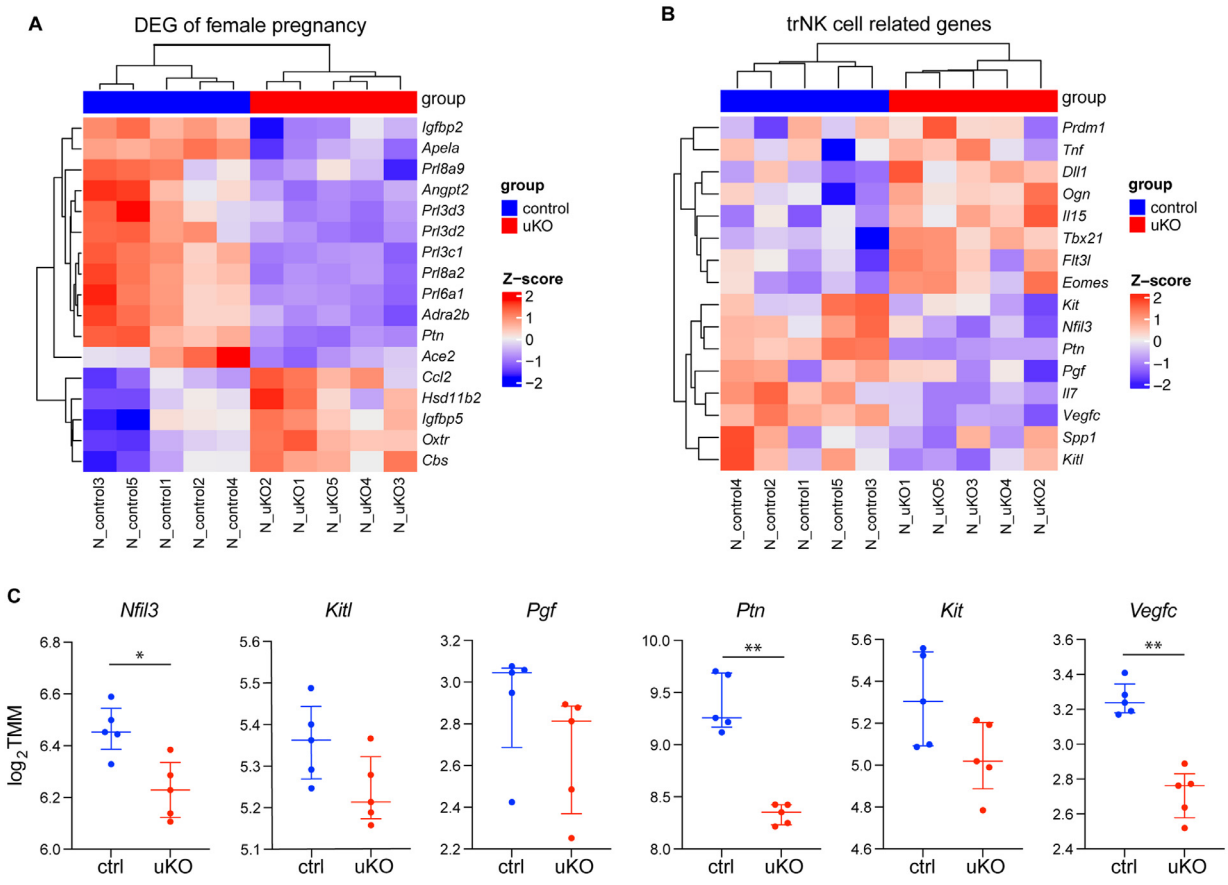

Fig. 8. Comparative transcriptomic analysis of implantation sites at day 6.

(A) Relative expression of DEG in GO term "female pregnancy." (B) Relative expression of trNK cell-related genes. (C) Comparison of expression levels of key genes in (B). Differences were analyzed using Mann-Whitney test; median ± interquartile range; $*p < 0.05$, $**p < 0.01$.

ctrl, control mice; uKO, uterine-specific *Vcan* deletion mice.

cell-related gene set could distinguish ctrl and uKO, suggesting these molecules are involved in the impaired proliferation of trNK cells. Among them, *Nfil3, KitL*, and *Pgf* [6,23-25], associated with uterine NK activation and differentiation, may contribute to the mechanism of poor proliferation.

A limitation of this study is that we could not perform functional experiments using human samples. In humans, NK cells express tissue-resident marker CD49a and exist abundantly in decidua [33], and are involved in the dilation of spiral arteries, promotion of trophoblast invasion, and immunotolerance [12,34]. Although we could not directly demonstrate the involvement of versican in NK cell proliferation in humans, immunostaining patterns of versican and localization of NK cells in the versican-rich region in early pregnancy in humans and mice suggest that versican contributes to spiral artery modification and placental formation in humans as in mice.

In conclusion, our study provides a new paradigm that the microenvironment of decidua with versican contributes to NK cell proliferation and spiral artery dilatation, required for fetal growth.

Experimental procedures

Human implantation sites and placenta tissue sample

Tissue sample of human embryo implantation site was collected from therapeutic hysterectomies for cervical cancer at 10 weeks of gestation ($n = 1$), and placentas were obtained from legal abortions of normal pregnancies at 18 and 21 weeks of gestation ($n = 2$) and infection-free cesarean section cases at 30 weeks ($n = 2$). Informed consent for the use of these samples was obtained from each donor. The use of these samples was also approved by the Ethical Committee of Kyoto University Hospital (R2949−1).

Animals (*Vcan* deletion mice and V1R mice)

Animal care and experimental procedures were performed under approval from the Institutional Animal Care and Use Committee and the DNA Recombination Experiment Safety Committee of Kyoto University. WT mice (C57BL/6, Japan SLC), *Vcan*-floxed mice [35], *Pgr*-Cre mice [36], and V1R mice [37] were used in this study. *Vcan*-floxed mice and V1R mice were provided by Hideto Watanabe (Institute for Molecular Science of Medicine, Aichi Medical University, Japan), and *Pgr*-Cre mice were provided by John P. Lydon and Francesco J. DeMayo (Baylor College of Medicine, USA). We generated uterine-specific *Vcan* deletion mice (uKO mice: *Pgr* cre/wt; *Vcan* flox/flox) by mating *Pgr*-Cre mice and *Vcan*-floxed mice. Cre-negative homozygous littermates (*Pgr* wt/wt; *Vcan* flox/flox) were used as control mice (Supplemental Fig. 2A) [38].

Analysis of pregnancy outcome in uKO mice

To evaluate pregnancy outcome, 8- to 12-week-old female control and uKO mice were mated with 2- to 10-month-old fertile WT male mice. Day 1 of pregnancy was defined as recognizing the vaginal plug. At day 18, we performed cesarean sections and examined the pregnancy rate, the miscarriage rate, and the size and weight of the pups and placentas. In addition, maternal systolic blood pressure was measured by a noninvasive blood pressure monitor (MK-2000ST, Muromachi Kikai, Tokyo, Japan), and urinary albumin was measured by LBIS Mouse Urinary Albumin Assay Kit (FUJIFILM Wako Shibayagi, Tokyo, Japan).

H&E staining and immunostaining

Frozen sections of murine implantation sites were prepared as described previously [39,40]. For immunostaining, we used antibodies shown in Supplemental Table 2. For immunostaining of versican in murine uteri, pretreatment with chondroitinase ABC (1 milliunit/μL; C3667, Sigma-Aldrich, St. Louis, USA) for 45 min was required [35]. Images were photographed by fluorescence microscope (BZ-9000, Keyence, Chicago, USA) and Optical microscope (BX51 and DP-20, Olympus, Tokyo, Japan).

Analysis of implantation sites

Quantification was performed using QuPath (Ver. 0.2.3) and ImageJ (Ver. 1.52k) software. The size of the decidua was quantified as a ratio to the entire placental area, including the myometrium, and the depth of MLAp was calculated as a ratio to the whole placental depth, including the myometrium [23]. For the evaluation of spiral arteries at days 10 and 14, we calculated the ratio of the lumen diameter to the wall diameter for multiple spiral arteries, which was used as an index of spiral artery modification [21,41]. The area of the lateral vascular space (LVS) at day 8 was calculated using ImageJ by drawing a border on the lumen of the LVS using QuPath. Antimesometrial decidual zone ratio was calculated as the ratio of the depth of decidualized cells to that of the entire endometrial stromal cell layer depth on the antimesometrial side [27].

qRT-PCR

Total RNA was extracted using TRIzol (Thermo Fisher Scientific, Waltham, USA). First Strand cDNA Synthesis Kit (GE Healthcare, Piscataway, USA) was used for cDNA synthesis. Real-time quantitative PCR was carried out by amplifying the target gene and reference genes with StepOnePlus (Thermo Fisher Scientific, Waltham, USA). Relative mRNA expression levels were estimated using the ΔΔCt method [39], and were normalized to β actin. Primers utilized in real-time q-PCR are shown in Supplemental Table 3.

Flow cytometry

Decidual capsules were removed from the uterine wall, and four or more littermate implantation sites were pooled at days 6, 8, and 10 for both uKO and control mice. Though conceptuses were not removed at day 6, conceptuses and antimesometrium were removed at days 8 and 10. Decidua was processed into single-cell suspensions using a modification of a previously published technique [23,42]. Samples were blocked using anti-CD16/CD32 antibody (101,301, BioLegend San Diego, USA), then were incubated with antibodies listed in Supplemental Table 4 for 40 min on ice. Antibodies listed in Supplemental Table 5 were used with Foxp3/Transcription Factor Staining buffer (00−5523−00, eBiosciense San Diego, USA) for staining of Ki67 and DAPI. For evaluating proliferation, Bromodeoxyuridine (BrdU) in sterile saline solution at 100 mg BrdU/kg was injected intraperitoneally into day 6 mice at 9 AM, and implantation sites were collected at 11 AM. Antibodies listed in Supplemental Table 6 were used with a BrdU Staining Buffer set (00−5525−00, eBioscience, San Diego, USA). Labeling was assessed using MACS Quant (Miltenyi Biotec, Bergisch Gladbach, Germany).

Comparative transcriptomic analysis of implantation sites

Two implantation sites without myometrium per mouse at day6 were collected from the control and uKO mice (n = 5). From those tissues, RNA was extracted using the PureLink RNA mini Kit (Thermo Fisher Scientific, Waltham, USA). Libraries were

prepared with the TruSeq stranded mRNA LT Sample Prep Kit (Illumina) and sequenced with the NovaSeq6000 (Illumina). Trimmed reads using Trimmomatic 0.38. were mapped to the reference genome, mm10, with HISAT2 version 2.1.0. After the read mapping, StringTie version 2.1.3b was used for transcript assembly. All expressed genes were defined as genes whose mapped read counts were >0 in all samples. The read count data was normalized with Trimmed mean of M-values (TMM) method in edgeR library. Then, statistical tests were performed with the normalized data. DEG (Differentially Expressed Genes) was defined as satisfied | fold change|$>$=2 & exactTest raw p-value$<$0.05. GO term analysis was performed in gProfiler with the term size set to 10$-$500.

Statistical analysis

Two-group comparisons were performed using two-sided Mann-Whitney tests, multiple Mann-Whitney tests, and the Kruskal-Wallis test, followed by Dunn's multiple comparison test. Data were presented as median with an interquartile range. All statistical analyses were performed using GraphPad Prism 8 (GraphPad Software, La Jolla, CA, USA). Values of $p < 0.05$ and Q-values of < 0.01 were considered significant.

Author contributions

Author contributions: YS, AH, HT conceived the study and designed experiments; YS, AY, TO, BN, YK performed the experiments; YS, AH, AO performed interpretation of data, YS, AH, HW drafted the paper, AH, KY, JH, TD, MM conducted review and revisions; JPL, FJD, TD, HW contributed to the design and provided resources.

Data Availability

Data will be made available on request.

Competing Interests statement

The authors declare no conflicts of interest associated with this manuscript.

Acknowledgments

This work was supported by grants from KAKENHI (17K11231) and the Takeda Science Foundation. The generation of the *Pgr*-Cre mouse was supported by NIH/NICHD grant (R01 HD042311 to JPL).

Supplementary materials

Supplementary material associated with this article can be found in the online version at doi:10.1016/j.matbio.2022.11.004.

Received 2 August 2022;
Received in revised form 17 November 2022;
Accepted 20 November 2022
Available online 21 November 2022

Keywords:
Versican;
Extracellular matrix;
Uterine NK cell;
Spiral artery;
Fetal growth restriction;
Preeclampsia

Abbreviations:
cNK cells, conventional NK cells; CS, chondroitin sulfate; ECM, extracellular matrix; EVT, extravillous trophoblast; HA, hyaluronan; LVS, lateral vascular sinus; MLAp, the mesometrial lymphoid aggregate of pregnancy; trNK cells, tissue-resident NK cells

References

[1] Y. Sang, Y. Li, L. Xu, D. Li, M. Du, Regulatory mechanisms of endometrial decidualization and pregnancy-related diseases, Acta Biochim Biophys Sin (Shanghai) 52 (2) (2020) 105–115.
[2] A.C. Staff, The two-stage placental model of preeclampsia: an update, J. Reprod. Immunol. 134-135 (2019) 1–10.
[3] J. Cha, X. Sun, S.K. Dey, Mechanisms of implantation: strategies for successful pregnancy, Nat. Med. 18 (12) (2012) 1754–1767.
[4] S.W. Ng, G.A. Norwitz, M. Pavlicev, T. Tilburgs, C. Simon, E.R. Norwitz, Endometrial decidualization: the primary driver of pregnancy health, Int. J. Mol. Sci. 21 (11) (2020).
[5] N.J. Hannan, L.A. Salamonsen, CX3CL1 and CCL14 regulate extracellular matrix and adhesion molecules in the trophoblast: potential roles in human embryo implantation, Biol. Reprod. 79 (1) (2008) 58–65.
[6] B. Fu, Y. Zhou, X. Ni, X. Tong, X. Xu, Z. Dong, et al., Natural killer cells promote fetal development through the secretion of growth-promoting factors, Immunity 47 (6) (2017) 1100-13 e6.
[7] D.K. Sojka, L. Yang, W.M. Yokoyama, Uterine natural killer cells: to protect and to nurture, Birth Defects Res. 110 (20) (2018) 1531–1538.
[8] D.K. Sojka, L. Yang, W.M. Yokoyama, Uterine natural killer cells, Front Immunol. 10 (2019) 960.
[9] S. Chantakru, C. Miller, L.E. Roach, W.A. Kuziel, N. Maeda, W.C. Wang, et al., Contributions from self-renewal and

trafficking to the uterine NK cell population of early pregnancy, J. Immunol. 168 (1) (2002) 22–28.
[10] A.A. Ashkar, G.P. Black, Q. Wei, H. He, L. Liang, J.R. Head, et al., Assessment of requirements for IL-15 and IFN regulatory factors in uterine NK cell differentiation and function during pregnancy, J. Immunol. 171 (6) (2003) 2937–2944.
[11] A.A. Ashkar, J.P. Di Santo, B.A. Croy, Interferon gamma contributes to initiation of uterine vascular modification, decidual integrity, and uterine natural killer cell maturation during normal murine pregnancy, J. Exp. Med. 192 (2) (2000) 259–270.
[12] S.D. Smith, C.E. Dunk, J.D. Aplin, L.K. Harris, R.L. Jones, Evidence for immune cell involvement in decidual spiral arteriole remodeling in early human pregnancy, Am. J. Pathol. 174 (5) (2009) 1959–1971.
[13] Y. Miyazaki, A. Horie, H. Tani, M. Ueda, A. Okunomiya, K. Suginami, et al., Versican V1 in human endometrial epithelial cells promotes BeWo spheroid adhesion in vitro, Reproduction (2018).
[14] Croy A. The guide to investigation of mouse pregnancy. Available from: https://yale.idm.oclc.org/login?URL=https://ebookcentral.proquest.com/lib/yale-ebooks/detail.action?docID=1579278.
[15] T.N. Wight, Provisional matrix: a role for versican and hyaluronan, Matrix Biol. 60-61 (2017) 38–56.
[16] S. Islam, Watanabe H. Versican, A dynamic regulator of the extracellular matrix, J. Histochem. Cytochem. 68 (11) (2020) 763–775.
[17] P. Kischel, D. Waltregny, B. Dumont, A. Turtoi, Y. Greffe, S. Kirsch, et al., Versican overexpression in human breast cancer lesions: known and new isoforms for stromal tumor targeting, Int. J. Cancer 126 (3) (2010) 640–650.
[18] A. Masuda, H. Yasuoka, T. Satoh, Y. Okazaki, Y. Yamaguchi, M. Kuwana, Versican is upregulated in circulating monocytes in patients with systemic sclerosis and amplifies a CCL2-mediated pathogenic loop, Arthritis Res. Ther. 15 (4) (2013) R74.
[19] K. Suwan, K. Choocheep, S. Hatano, P. Kongtawelert, K. Kimata, H. Watanabe, Versican/PG-M assembles hyaluronan into extracellular matrix and inhibits CD44-mediated signaling toward premature senescence in embryonic fibroblasts, J. Biol. Chem. 284 (13) (2009) 8596–8604.
[20] T.N. Wight, I. Kang, M.J. Merrilees, Versican and the control of inflammation, Matrix Biol. 35 (2014) 152–161.
[21] B.A. Croy, J. Zhang, C. Tayade, F. Colucci, H. Yadi, A.T. Yamada, Analysis of uterine natural killer cells in mice, Methods Mol. Biol. 612 (2010) 465–503.
[22] D.K. Sojka, L. Yang, B. Plougastel-Douglas, D.A. Higuchi, B.A. Croy, W.M. Yokoyama, Cutting edge: local proliferation of uterine tissue-resident NK cells during decidualization in mice, J. Immunol. 201 (9) (2018) 2551–2556.
[23] S. Boulenouar, J.M. Doisne, A. Sferruzzi-Perri, L.M. Gaynor, J. Kieckbusch, E. Balmas, et al., The residual innate lymphoid cells in NFIL3-deficient mice support suboptimal maternal adaptations to pregnancy, Front. Immunol. 7 (2016) 43.
[24] X. Ni, B. Fu, J. Zhang, R. Sun, Z. Tian, H. Wei, Cytokine-based generation of CD49a(+)Eomes(-/+) natural killer cell subsets, Front. Immunol. 9 (2018) 2126.
[25] C. Tayade, D. Hilchie, H. He, Y. Fang, L. Moons, P. Carmeliet, et al., Genetic deletion of placenta growth factor in mice alters uterine NK cells, J. Immunol. 178 (7) (2007) 4267–4275.
[26] J.B. Pawlak, L. Balint, L. Lim, W. Ma, R.B. Davis, Z. Benyo, et al., Lymphatic mimicry in maternal endothelial cells promotes placental spiral artery remodeling, J. Clin. Invest. 129 (11) (2019) 4912–4921.
[27] M.L. Redhead, N.A. Portilho, A.M. Felker, S. Mohammad, D.L. Mara, B.A. Croy, The transcription factor NFIL3 Is essential for normal placental and embryonic development but not for uterine natural killer (UNK) cell differentiation in mice, Biol. Reprod. 94 (5) (2016) 101.
[28] C.H. Mjaatvedt, H. Yamamura, A.A. Capehart, D. Turner, R.R. Markwald, The Cspg2 gene, disrupted in the hdf mutant, is required for right cardiac chamber and endocardial cushion formation, Dev. Biol. 202 (1) (1998) 56–66.
[29] S. Nandadasa, A. O'Donnell, A. Murao, Y. Yamaguchi, R.J. Midura, L. Olson, et al., The versican-hyaluronan complex provides an essential extracellular matrix niche for Flk1(+) hematoendothelial progenitors, Matrix Biol. 97 (2021) 40–57.
[30] H. Yamamura, M. Zhang, R.R. Markwald, C.H. Mjaatvedt, A heart segmental defect in the anterior-posterior axis of a transgenic mutant mouse, Dev. Biol. 186 (1) (1997) 58–72.
[31] T.D. Camenisch, A.P. Spicer, T. Brehm-Gibson, J. Biesterfeldt, M.L. Augustine, A. Calabro Jr., et al., Disruption of hyaluronan synthase-2 abrogates normal cardiac morphogenesis and hyaluronan-mediated transformation of epithelium to mesenchyme, J. Clin. Invest. 106 (3) (2000) 349–360.
[32] K. Spiess, W.R. Teodoro, T.M. Zorn, Distribution of collagen types I, III, and V in pregnant mouse endometrium, Connect. Tissue Res. 48 (2) (2007) 99–108.
[33] R. Vento-Tormo, M. Efremova, R.A. Botting, M.Y. Turco, M. Vento-Tormo, K.B. Meyer, et al., Single-cell reconstruction of the early maternal-fetal interface in humans, Nature 563 (7731) (2018) 347–353.
[34] P. Vacca, L. Chiossone, M.C. Mingari, L. Moretta, Heterogeneity of NK cells and other innate lymphoid cells in human and murine decidua, Front. Immunol. 10 (2019) 170.
[35] K. Choocheep, S. Hatano, H. Takagi, H. Watanabe, K. Kimata, P. Kongtawelert, et al., Versican facilitates chondrocyte differentiation and regulates joint morphogenesis, J. Biol. Chem. 285 (27) (2010) 21114–21125.
[36] S.M. Soyal, A. Mukherjee, K.Y. Lee, J. Li, H. Li, F.J. DeMayo, et al., Cre-mediated recombination in cell lineages that express the progesterone receptor, Genesis 41 (2) (2005) 58–66.
[37] S. Islam, K. Chuensirikulchai, S. Khummuang, T. Keratibumrungpong, P. Kongtawelert, W. Kasinrerk, et al., Accumulation of versican facilitates wound healing: implication of its initial ADAMTS-cleavage site, Matrix Biol. 87 (2020) 77–93.
[38] L. Matsumoto, Y. Hirota, T. Saito-Fujita, N. Takeda, T. Tanaka, T. Hiraoka, et al., HIF2alpha in the uterine stroma permits embryo invasion and luminal epithelium detachment, J. Clin. Invest. 128 (7) (2018) 3186–3197.
[39] M. Ueda, Y. Sato, A. Horie, H. Tani, Y. Miyazaki, A. Okunomiya, et al., Endovascular trophoblast expresses

CD59 to evade complement-dependent cytotoxicity, Mol. Cell. Endocrinol. 490 (2019) 57–67.

[40] Y. Sato, H. Fujiwara, B.X. Zeng, T. Higuchi, S. Yoshioka, S. Fujii, Platelet-derived soluble factors induce human extravillous trophoblast migration and differentiation: platelets are a possible regulator of trophoblast infiltration into maternal spiral arteries, Blood 106 (2) (2005) 428–435.

[41] J. Kieckbusch, L.M. Gaynor, F. Colucci, Assessment of maternal vascular remodeling during pregnancy in the mouse uterus, J. Vis. Exp. (106) (2015) e53534.

[42] B.A. Croy, Z. Chen, A.P. Hofmann, E.M. Lord, A.L. Sedlacek, S.A. Gerber, Imaging of vascular development in early mouse decidua and its association with leukocytes and trophoblasts, Biol. Reprod. 87 (5) (2012) 125.